



ISTITUTO NAZIONALE DI RICERCA METROLOGICA Repository Istituzionale

Spectroscopic Characterization of Ti Sites in MWW Zeolite in Presence of Hydrogen Peroxide

This is the author's accepted version of the contribution published as:

Original

Spectroscopic Characterization of Ti Sites in MWW Zeolite in Presence of Hydrogen Peroxide / Rosso, F., Airi, A., Signorile, M., Bordiga, S., Crocellà, V., Bonino, F.. - In: CHEMCATCHEM. - ISSN 1867-3899. - (2024). [10.1002/cctc.202301653]

Availability:

This version is available at: 11696/83359 since: 2025-01-23T09:04:28Z

Publisher:

WILEY-V C H VERLAG GMBH

Published

DOI:10.1002/cctc.202301653

Terms of use:

This article is made available under terms and conditions as specified in the corresponding bibliographic description in the repository

Publisher copyright
WILEY POST PRINT

This article may be used for non-commercial purposes in accordance with Wiley Terms and Conditions for Use of Self-Archived Versions. This article may not be enhanced, enriched or otherwise transformed into a derivative work, without express permission from Wiley or by statutory rights under applicable legislation. Copyright notices must not be removed, obscured or modified. The article must be linked to Wiley's

(Article begins on next page)

Spectroscopic Characterization of Ti Sites in MWW Zeolite in Presence of Hydrogen Peroxide

Francesca Rosso,¹ Alessia Airi,^{1,2} Matteo Signorile,¹ Silvia Bordiga,¹ Valentina Crocellà,¹ Francesca Bonino^{1*}

¹ Department of Chemistry, NIS and INSTM Reference Centre, Università di Torino, Via G. Quarello 15, 10135 and Via P. Giuria 7, 10125, Torino, Italy.

² Present address: INRiM Istituto Nazionale di Ricerca Metrologica, Strada delle cacce 91 I-10135, Turin, Italy.

Abstract

Ti-MWW zeolite is a promising catalyst for partial oxidation reactions. In the present work, a Ti-MWW sample with high TiO₂ loading was synthesized. It was revealed that the Ti insertion in the purely siliceous MWW framework mainly occurs during the post treatment washing with HNO₃, when the double structure directing agent synthetic method is used. By exploiting carbon monoxide, acetonitrile, pyridine and ammonia as probe molecules in infrared spectroscopy and diffuse reflectance ultraviolet spectroscopy, the acidic behavior of the Ti sites and the interaction of the Ti sites with hydrogen peroxide (H₂O₂) were revealed. The Ti Lewis acid sites showed stronger acidity than the one observed in Titanium Silicalite-1 (TS-1), with MFI framework. This is coherent with previously reported results, suggesting that a significative fraction of the Ti sites in Ti-MWW are TiOH(SiO)₃ instead of Ti(OSi)₄. The Ti-peroxo and -hydroperoxo complexes formed upon H₂O₂ were shown to be more labile than in TS-1 and they were shown to be completely reversible upon calcination.

Introduction

Titanium (Ti) doped zeolites are used as shape selective catalysts for partial oxidation reactions (e.g. epoxidations¹⁻⁶ or hydroxylations⁷⁻¹⁰), using hydrogen peroxide (H₂O₂) as oxidizing agent.^{1,11} A small percentage (2-3%) of silicon (Si) atoms are isomorphously substituted by Ti in the zeolite structure, in absence of other heteroatoms. The isomorphous substitution of Ti provides uncoordinated sites that adsorb H₂O₂ and form Ti-hydroperoxo (Ti-OOH) or -peroxo (Ti-OO⁻) complexes.¹² The transfer of an active oxygen (O) to the organic substrate, with production of a water (H₂O) molecule, ends the catalytic cycle.

The most renowned Ti-zeolite is the Titanium Silicalite-1 (TS-1)¹³ with a MFI framework, discovered in 1983 and still the best known and most studied system. From the TS-1 discovery many efforts were made to enhance the performances of Ti-zeolites in the same target reaction. These include refining the properties of

the catalyst¹⁴⁻²⁷ or acting on the reaction conditions.^{7,28-30} Among the former, modifications of the synthetic procedures to improve the amount and speciation of Ti,^{11,31-38} diffusion boosting with additional porosity levels¹⁵⁻¹⁹ and changes of the crystalline zeolitic framework^{14,20-22,27,39} are the most important. In this work, the attention was focused on Ti-zeolites with MWW framework (Ti-MWW) which have recently been showing very promising catalytic outcomes, tested in many partial oxidation reactions.^{5,6,27,40} MWW is a layered framework type^{41,42} and hosts two independent pore systems. 10 Member-Ring (MR) sinusoidal channels (diameter of 5.2 Å) run intralayer and a system of internal super-cages with dimension of 7.1 Å x 18.2 Å is located in the interlayer space, connected to the outside via 10 MR apertures. The super-cages are cut at the crystal external surface and form hemi-cages, that catalytically behave as 12 MR channels (7.1 Å diameter). The 12 MR hemi-cages impose the same shape selectivity of a 12 MR channel without the need of diffusing reagents and products in real channels and hence hindering the deactivation by coke formation.^{41,43-45} Ti-MWW was first synthesized in 2001, in co-presence of boron (B) and Ti.⁴⁴ Subsequently, a deboronation procedure and a direct synthesis of Ti-MWW in absence of B were developed,^{27,46} to obtain materials without additional catalytic sites, except for Ti. The Ti insertion in the MWW framework is reported to occur in the vacant sites formed during the deboronation by acid washing of the Ti-B-MWW⁴⁶ and an acid treatment is also necessary after the direct synthesis of Ti-MWW, to remove the extra-framework anatase.²⁷ Here, a deep study of the effect of the acid treatment on the directly synthesized Ti-MWW is reported and the role of the acid treatment in the formation of Ti active sites is unveiled.

The increasing attention for this catalytic system imposes to reach a clear understanding of the Ti-MWW active sites, as has already been done for a long time with the well-known TS-1 case. Indeed, during the years an in-depth knowledge of the active sites and species in TS-1 has been achieved. For TS-1, the Ti insertion can occur in substitutional “perfect” tetrahedral sites, in octahedral coordination as bulk anatase or in the so-called “amorphous” Ti species (i.e. intermediate conditions between the previously described, e.g. hexacoordinated, in a distorted octahedral geometry, maybe in the presence of alkali metal cations) depending on the synthetic procedure and Ti loading.^{4,34,35,47} The Ti sites in TS-1 showed preferential location in specific crystallographic sites, and both the speciation and location were extensively studied by spectroscopy,^{34,47-53} diffraction⁵⁴⁻⁵⁶ and computational methods.^{47,50,53,57-59} The knowledge gained by studying TS-1 is very useful for understanding which active site must be pushed in synthetic studies and to design catalysts with different levels of porosity.³¹ However, when the crystalline framework is modified, the Ti microenvironment and, consequently, the behavior of the Ti-OOH and Ti-OO⁻ active species can be different, as in the case of Ti-MWW. The vibrational fingerprint that testifies the presence of “perfect” Ti sites Ti(OSi)₄ in Ti-zeolites (the band at 960 cm⁻¹ in the TS-1 vibrational spectrum),⁵³ in Ti-MWW is composed of two bands peaked at 960 and 930 cm⁻¹.^{27,44} This suggests the presence of different Ti microenvironments and computational studies^{27,60} confirm this hypothesis. The computational studies revealed the co-presence of Ti(OSi)₄ and TiOH(OSi)₃ species in comparable abundance in Ti-MWW and that TiOH(OSi)₃ locates selectively at the T1

crystallographic site. A commonly accepted view regarding the comparison among the catalytic activity of the different Ti sites is not achieved yet,^{1,61-64} but some studies⁶³⁻⁶⁵ report that TiOH(OSi)₃ are more active than Ti(OSi)₄ sites in epoxidation reactions. The reason of the possible higher activity of TiOH(SiO)₃ sites was ascribed to their stronger Lewis acidity compared to the one of Ti(OSi)₄ sites, but the experimental work published in this field⁶⁵ does not directly compare the two zeolitic frameworks for providing a complete description of the different activity of the sites generated in the two different frameworks. On the other side, the in-depth spectroscopical analysis of the Ti sites and of the formation of the Ti-OOH and Ti-OO⁻ complexes upon interaction with H₂O₂ is lacking. In this work, we present a combined synthetic and spectroscopical study of the acidic properties of the Ti-MWW catalyst and of its interaction with H₂O₂. The effect of the post-treatment washing with nitric acid (HNO₃) on the process of Ti insertion in the MWW framework was studied by comparing a washed and not washed Ti-MWW samples. A combination of vibrational (infrared, IR) and electronic (ultraviolet-visible, UV-Vis) spectroscopies, in presence of probe molecules, when necessary, was adopted to shed light on the reason of the catalytic behavior of Ti-MWW and to provide a direct means of comparison with TS-1.

Experimental Section

Chemicals

Aerosil® 200 (from Evonik Industries) and tetrabutylorthotitanate (TBOT, reagent grade 97% from Sigma Aldrich), were used as Si and Ti source. N,N,N-trimethyl-adamantyl-ammonium hydroxide (TMAdaOH, 25 wt% in water, from TCI), hexamethylenimine (HMI, 99% from Sigma Aldrich) were used as Organic Structure Directing Agent (OSDA); potassium carbonate (K₂CO₃, anhydrous, ACS reagent, from Sigma Aldrich) was used as additive for the synthesis; Milli-Q water (18.2 MΩ cm) was used as solvent and nitric acid (HNO₃, 65% for analysis-ISO, from Carlo Erba Reagents) was used for the washings of Ti-MWW samples. Hydrogen peroxide (H₂O₂) aqueous solution (≥ 30 %, for trace analysis, from Sigma Aldrich) was used as oxidizing agent.

Synthesis of the Ti-MWW sample

The preparation of the Ti-MWW sample was reproduced from Xu et al.²⁷ In a typical synthesis, 8.45 g of TMAdaOH solution, 1.49 g of HMI and 0.2416 g of K₂CO₃ were added to 20.68 g of Milli-Q water in this order. After the complete dissolution of K₂CO₃, 0.34 g of TBOT were added dropwise under vigorous stirring. The solution was stirred at room temperature for 30 min to allow complete hydrolysis of the Ti precursor and then 3.004 g of Aerosil® 200 were gradually added and the gel was stirred until it was fully homogeneous. The final composition of the synthesis gel was: 1 SiO₂ : 0.02 TiO₂ : 0.2 TMAdaOH : 0.3 HMI : 0.035 K₂CO₃ : 30 H₂O. The gel (approximately 30 ml) was then transferred to a 45 ml Teflon lined stainless steel digester and it was crystallized by autogenous pressure at 150 °C, in tumbling conditions at 60 rpm. The gel was filtered, washed

with abundant water and dried at 65 °C overnight (to obtain Ti-MWW-as, “as” meaning “as-synthesized”). A portion of Ti-MWW-as was washed with a 2 M HNO₃ solution for 20 h at 100 °C, under reflux conditions, using a solid to liquid ratio of 1 g : 50 ml, to obtain Ti-MWW-HNO₃-as. Ti-MWW-as and Ti-MWW-HNO₃-as were calcined at 550 °C under O₂ flow, using a heating ramp of 1 °C/min followed by 7 h of isotherm, to obtain Ti-MWW-calc and Ti-MWW-HNO₃-calc.

The reference ITQ-1 material was synthesized as described elsewhere,⁶⁶ using the following composition of the synthesis gel: 1 SiO₂ : 0.25 TMAOH : 0.31 HMI : 44 H₂O and calcined at 550 °C under air flow, using a heating ramp of 1 °C/min followed by 7 h of isotherm. ITQ-1-as and ITQ-1-calc are the references before and after the calcination, respectively.

Characterization techniques

Powder X-Rays Diffraction (PXRD) patterns were obtained using Cu K_α radiation, on a PANalytical X'Pert diffractometer (Bragg-Brentano geometry), equipped with a X'celerator strip detector, in the range 5° ≤ 2θ ≤ 45°, with a step of 0.02° and 50 s/° of integration. Cu K_β was suppressed with a Ni filter.

N₂ physisorption isotherms were recorded on a Micromeritics 3Flex instrument at -196 °C. The powders were treated before the measurement, by outgassing overnight at 120 °C and then 7 h at 400 °C. The Specific Surface Areas (SSAs) were determined by the Brunauer-Emmett-Teller (BET) and Langmuir models, applied in pressure ranges suitable for obtaining a monolayer capacity included in the selected p/p⁰ (for the BET) or p (for the Langmuir) linearization range.⁶⁷ The cumulative pore volume and the pore size distribution were obtained by applying the Non-Local Density Functional Theory (NL-DFT); the pores were modelled as slit pores, using the “N₂@ 77-Carbon, original DFT” available in the Microactive software.⁶⁸ The model was applied in the whole range of p/p⁰ with a regularization of 10⁻².

The TiO₂ wt% was determined by an Energy Dispersive X-Rays (EDX) spectroscopy detector (Oxford – Detector, equipped with an AZTEC software) coupled with a Field Emission (FE) Scanning Electron Microscope (SEM) Tescan S9000G. Areas that contain exclusively zeolitic particles were carefully selected. Elemental maps were acquired in the same condition. Four areas were analysed for each sample.

The TiO₂ wt% was also determined by an Optical Emission Spectroscopy (OES) detector equipped with an Inductively Coupled Plasma (ICP) source from Perkin Elmer (7000 DV), cross-flow nebulizer, Scott nebulization chamber and an Echelle monochromator. The dissolution was performed three times for each sample on 30 mg aliquots, in a microwave oven (1200 MEGA from Milestone), using 5 ml of aqua regia and 2 ml of HF. A second dissolution was performed adding 0.7 g of H₃BO₃, in a final volume of 25 ml. Three replicas were performed for each sample.

Diffuse Reflectance (DR) Ultraviolet-visible (UV-Vis) spectra were collected on a Varian Cary5000 spectrophotometer, using Spectralon® as 100% Reflectance reference. The samples were measured both as such and after a pretreatment for removing water and possible organic pollutants on Ti coordination (the procedure is referred as “activation” in the following). ≈ 50 mg of sample were inserted in a quartz tube suitable for high temperature in vacuo treatments and the same portion of sample was analyzed by UV-Vis and by Attenuated Total Reflectance (ATR) Infrared (IR) (described later) spectroscopies. The procedure involves outgassing the sample at room temperature (RT) until reaching the residual pressure of $< 10^{-3}$ mbar; then the samples were heated up to 500 °C with a 5 °C/min ramp. After 30 min of outgassing at 500 °C, 100 mbar of pure O₂ were dosed on the sample and left in contact for at least 30 min. O₂ was finally outgassed and the temperature was kept at 500 °C till a residual pressure $< 5 \times 10^{-4}$ mbar (≈ 1 h). After cooling to RT, the quartz tube was transferred in a N₂ glove-box for filling the sample holder for UV-Vis spectroscopy under controlled atmosphere.

The Attenuated Total Reflectance (ATR)-IR spectra were collected on a Bruker Alpha II spectrophotometer located directly inside the N₂ glove-box on the same fraction of sample activated for the UV-Vis measurements. The spectrophotometer is equipped with a Deuterated TriGlycine Sulfate (DTGS) detector and an ATR Platinum accessory (internal reflection element made of diamond). 64 scans were mediated (128 for the background) and a resolution of 2 cm⁻¹ was used.

The transmission IR spectra were collected with a Bruker Vertex 70 spectrophotometer, equipped with a Mercury Cadmium Telluride (MCT) cryo-detector on a self-supporting pellet of the pure sample, placed inside a home-made quartz cell with KBr windows, designed for thermal outgassing prior to the measurement. The pellet was mechanically protected by a gold envelope and activated as previously described. The spectra were acquired under vacuum accumulating 32 scans (64 for the background) at 2 cm⁻¹ of resolution.

The acidic properties of Ti-MWW-HNO₃-calc and the reference ITQ-1-calc were studied by dosing gaseous basic probe molecules on the sample under acquisition, by connecting the home-made cell (equipped with KBr or CaF₂ windows depending on the probe) to a vacuum glass-line. The spectral changes were detected during the adsorption/desorption of carbon monoxide (CO),^{69,70} deuterated acetonitrile (CD₃CN),⁷¹ pyridine (Py)⁷¹ and ammonia (NH₃)⁴⁸. The specific experimental settings for each molecule are reported elsewhere.^{48,69–71}

The interaction of H₂O₂ with the Ti sites in Ti-MWW-HNO₃-calc was studied in situ by UV-Vis and IR spectroscopies. The powder was put in contact with H₂O₂ aqueous solution, rapidly dried (≈ 20 min in air at RT) and milled to obtain a pale orange powder. The orange powder was left aging consecutively for 24 and 96 h and then was again put in contact with H₂O₂. After further 24 h aging the powder was regenerated by calcination in a tubular oven, with a heating ramp of 1 °C/min, at 550 °C for 4 h, under dry air flow. UV-Vis

spectra were recorded after each step. Parallely, the degradation of the complexes for short-elapse times (2, 3 and 4 h) was followed and finally the effect of contact with H₂O was observed.

The interaction with H₂O₂ was studied by IR spectroscopy in transmission mode (same parameters and equipment described before) by wetting a pellet with a drop of H₂O₂, drying it rapidly in air at RT (till the residues of solution were not visible on the surface by naked eye) and then placing it in an IR cell with KBr windows. The pellet was quickly outgassed, to remove the air and the excess of water. Then, 40 mbar of pure propylene were dosed on the sample to observe the formation of propylene oxide. The spectra of propylene and propylene oxide dosed on the sample without H₂O₂, were recorded as reference. CD₃CN was also dosed on the H₂O₂ soaked and rapidly outgassed sample to verify that CD₃CN could not interact with Ti sites when they are already interacting with H₂O₂.

Results and Discussion

Crystalline structure and defects analysis

The PXRD diffractograms of the as-synthesized ITQ-1-as, Ti-MWW-as and Ti-MWW-HNO₃-as and calcined ITQ-1-calc, Ti-MWW-calc and Ti-MWW-HNO₃-calc samples are shown in Figure 1. The position and bandwidth of the reflections is coherent with what reported in literature^{27,41,66,72} and the presence of different zeolitic phases or of bulk anatase (in Ti containing samples) in detectable amounts is excluded. The calcined samples show shifted (among others, 002, 101 and 102) and fixed (e.g. the 100) reflections, compared with the as-synthesized samples. The shifted reflections have a component along the *c* direction and their shift is due to the contraction of the *c* axis of the unit cell that occurs upon calcination.^{27,41,66,72} E.g. the 002 reflection shifts from 6.5° in Ti-MWW-as to 7.26° in Ti-MWW-calc and Ti-MWW-HNO₃-calc, overlapped to the nearby 100 reflection. The diffractogram of Ti-MWW-HNO₃-as reveals an intermediate state, since the 002 reflection is shifted and overlapped to 100, being the peak broad and asymmetrical. This suggests that the partial elimination of the OSDA starts already during the HNO₃ washing, as observed before⁷³ and testified also by the IR spectra reported in Figure S1.⁷³ The slight peak broadening, observed upon the acid treatment suggests a possible etching of the crystals or the reduction of the crystallite size. The SSA and micropore volume of Ti-MWW-calc are lower compared to ITQ-1-calc and Ti-MWW-HNO₃-calc (Table 1), as also visible at a first glance from the comparison of the N₂ isotherms (Figure S2, S3), suggesting a possible partial occlusion of the Ti-MWW-calc microchannels.

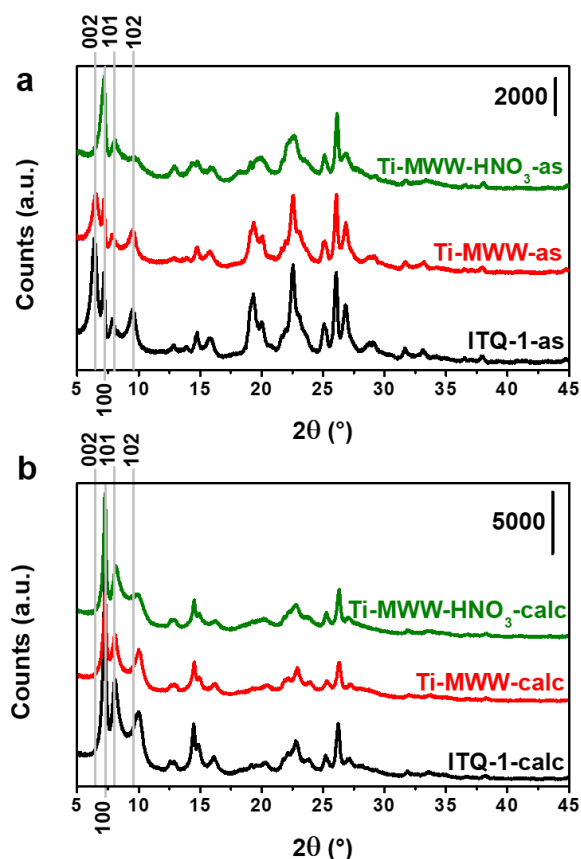


Figure 1. PXRD diffractograms in the 5° to 45° 2 θ range. (a) As-synthesized samples: ITQ-1-as (black), Ti-MWW-as (red) and Ti-MWW-HNO₃-as (olive). (b) Calcined samples: ITQ-1-calc (black), Ti-MWW-calc (red) and Ti-MWW-HNO₃-calc (olive). The vertical light gray lines refer to the position of the 002, 100, 101 and 102 reflections of samples ITQ-1-as and Ti-MWW-as both in *a* and *b* directions. The diffractograms are vertically shifted for sake of clarity.

Table 1. SSAs calculated with the BET and Langmuir models and micropore (V_{micro}) volume computed using the NL-DFT method.

Sample	BET SSA ¹ (m ² /g)	Langmuir SSA ² (m ² /g)	V_{micro} ³ (cm ³ /g STP)
ITQ-1-calc	465 ± 2	525 ± 1	0.15
Ti-MWW-calc	350 ± 2	384 ± 1	0.10
Ti-MWW-HNO ₃ -calc	498 ± 1	581 ± 2	0.15

¹ Calculated in the 0.008 – 0.08 p/p⁰ range.

² Calculated in the 15 – 200 mbar pressure range.

³ Calculated from the cumulative pore volume plot for pores size < 20 Å.

The effect of the HNO₃ washing on the calcination is also visible in the hydroxyls stretching ($\nu(\text{OH})$) range of silanols (Si-OH) and/or titanols (Ti-OH) (see IR spectra of Figure 2 between 3800-3000 cm⁻¹).^{69,74–77} The sharp

absorption at 3747 cm^{-1} is due to external isolated -OH groups. At lower wavenumber, the absorption of -OH groups is affected by a progressively more complex net of H-bonds. Among others, the Si-OH chain terminal at 3733 cm^{-1} and the Si-OH nests, generated by one or more Si missing atoms (broad absorption around 3500 cm^{-1}) are evident. It is worth noting that, in Ti-MWW-calc, isolated Si(Ti)-OHs are the only species absorbing in this region, due to defect healing phenomenon occurring upon direct calcination. A new band at 3688 cm^{-1} appears in Ti-MWW-HNO₃-calc spectrum. This signal was rarely observed before in a study regarding the Ti-MCM-41,⁷⁸ and was tentatively assigned to Ti-OH groups. We will see below that the assignment of this component is a difficult task, due to the small difference between the $\nu(\text{OH})$ stretching frequency of Si(Ti)-OH species. Moreover, Ti-MWW-HNO₃-calc exhibits a comparable amount of defective species (silanol nest) to the reference ITQ-1-calc sample.

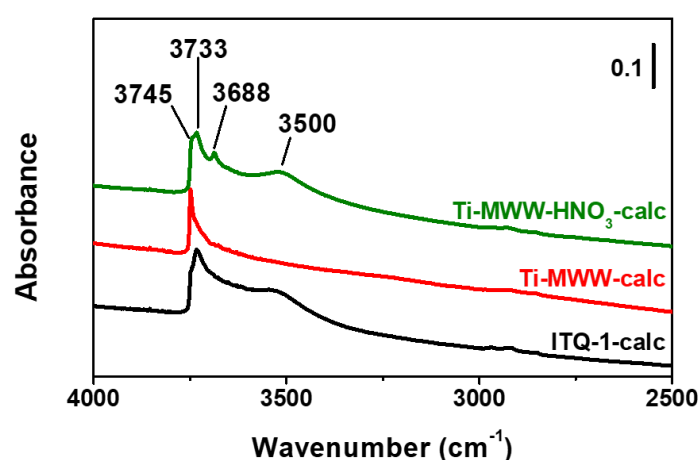


Figure 2. Transmission IR spectra of ITQ-1-calc (black), Ti-MWW-calc (red) and Ti-MWW-HNO₃-calc (olive) in the $4000\text{-}2500\text{ cm}^{-1}$ spectral range. The spectra are recorded after activation, internally normalized at the Si-O-Si stretching overtone absorptions, and vertically shifted for the sake of comparison.

Ti active site characterization

The limited amount of metal that can be inserted in Ti-zeolites is one of the main issues in the preparation and use of these catalysts. The TiO₂ content was determined by ICP-OES and SEM-EDX microanalysis (Table 2). The quantification in Ti-MWW-calc by ICP-OES shows that a loss of Ti species occurs during the hydrothermal crystallization: the Ti/Si molar ratio diminishes from 0.02 (nominal, used in the synthesis gel) to 0.012, probably due to the incomplete hydrolysis of the Ti source in the crystallization conditions.³¹ Moreover, the acid washing does not affect the amount of Si and Ti containing species in the sample. SEM-EDX is very useful for the internal comparison among the samples as it allows the microanalysis. In fact, the maps of the elemental distribution (Figures S4-S5) show the uniformity of the Ti incorporation and no differences between the acid washed and the directly calcined sample. The limit value for the framework tetrahedral Ti loading in TS-1 is around 2.5 wt% of TiO₂.^{4,79,80} and it was rarely obtained without the co-

presence of extra-framework species.^{31,81–86} The obtained TiO₂ loading for Ti-MWW-HNO₃-calc is an intriguing result, because it opens up the possibility of even higher loadings, considering that the higher limit for the MWW framework was not determined yet.

When SEM-EDX microanalysis is used, the TiO₂ content of Ti-MWW-HNO₃-calc (2.4 wt%) appears significantly higher than the one of Ti-MWW-calc (1.0 wt%). The Ti enrichment observed by microanalysis on the zeolitic lamellar sample could be due to the solubilization-recrystallization of not zeolitic, Ti-rich aggregates possibly present and not detected in the not washed sample. This is likely to happen because a loss of silicate species (that could have affected the Ti/Si ratio) is not detected by ICP-SEM. Hence, we do believe that Ti-rich aggregates formed in the hydrothermally synthesized sample, may be dissolved during the HNO₃ washing, providing available Ti species. The nature of such aggregates is unknown, but they could be related to the presence of potassium since it is present in Ti-MWW-calc and drastically reduced in Ti-MWW-HNO₃-calc (Table 2). The elemental maps support this last assumption (Figures S4-S5).

Table 2. Elemental analysis of Ti-MWW-calc and Ti-MWW-HNO₃-calc samples. The data are expressed as average ± standard deviation.

Sample	Ti/Si*	TiO ₂ (wt%)*	Ti/Si**	TiO ₂ (wt%)**	K (g/kg)*
Ti-MWW-calc	0.012 ± 0.03	1.5 ± 0.3	0.008 ± 0.001	1.0 ± 0.2	7 ± 2
Ti-MWW-HNO ₃ -calc	0.0128 ± 0.0002	1.67 ± 0.03	0.019 ± 0.001	2.4 ± 0.1	0.29 ± 0.01

* Determined by ICP-OES.

** Determined by SEM-EDX.

The spectroscopic characterization of the Ti sites in the two samples corroborates the hypothesis regarding the Ti insertion in Ti-MWW-HNO₃-calc. In the UV-Vis spectra (Figure 3a and Figures S6 and S7), the Ligand to Metal Charge Transfer (LMCT) electronic transition involving Ti is present. The band edge and maximum (visually the minimum when spectra are plotted in reflectance (%) scale) are sensitive to the environment around Ti atoms in the sample. For comparison, it must be considered that in fully dehydrated TS-1 samples, maxima at 210 nm and 310 nm testify the presence of “perfect” tetrahedral Ti sites and octahedrally coordinated Ti (anatase) respectively (Figure S6a).^{4,47} The presence of additional maxima between 210 and 310 nm is due to Ti species in intermediate conditions (e.g. isolated octahedral or distorted Ti species penta- or hexa-coordinated, see Figure S8a).^{4,34,35,47} In Ti-MWW the situation is analogue. Ti-MWW-HNO₃-calc shows a single band at 205 nm, doubtless assigned to framework tetrahedral Ti species.^{17,27,44} Ti-MWW-calc spectrum does not present any clear maximum around 210 nm, while a broad absorption at 235 nm with a shoulder at 280 nm is visible. This band can originate from intermediate Ti species in the framework and its wavelength is compatible with the LMCT in TiOH(OSi)₃ species.⁶⁴ The same signal is also slightly visible as shoulder in Ti-MWW-HNO₃-calc spectrum. However, it does not directly suggest that Ti-MWW-calc contains

more $\text{TiOH}(\text{OSi})_3$ species than in $\text{Ti-MWW-HNO}_3\text{-calc}$, considering that, a computational study revealed that, as an example, the $\text{Ti}(\text{OSi})_4$ and $\text{TiOH}(\text{OSi})_3$ species cannot be distinguished based on their UV-Vis spectrum.⁴⁷

The framework vibration region of the ATR-IR spectra is shown in Figure 3b. Here, in the transparency window ($990\text{-}850\text{ cm}^{-1}$), between the antisymmetric ($\nu_a(\text{SiOSi})=1100\text{ cm}^{-1}$) and symmetric ($\nu_s(\text{SiOSi})=800\text{ cm}^{-1}$) stretching bands, the $\nu_a(\text{SiOSi})$ vibrational mode, perturbed by the presence of Ti in the framework, is expected (see Figure S8b).⁵³ Ti-MWW-calc does not show bands in this region. Contrary, $\text{Ti-MWW-HNO}_3\text{-calc}$ spectrum reveals two bands at 965 and 930 cm^{-1} related to the presence of Ti atoms in slightly different environments.^{27,44} The first one is analogous, although slightly shifted to the band at 960 cm^{-1} present in dehydrated TS-1 and other Ti-zeolites (e.g. Ti-beta, Ti-CHA),^{20,36,39,51,87} and it testifies the presence of Ti atoms in tetrahedral coordination. The component at 930 cm^{-1} is typical of Ti-MWW catalysts^{27,44} and of some amorphous mesoporous silicates, as Ti-MCM-41, depending on the synthetic procedure.^{22,78} It was assigned to grafted Ti species ($\text{TiOH}(\text{OSi})_3$ or $\text{Ti}(\text{OH})_2(\text{SiO})_3$) in Ti-MCM-41⁷⁸ and to defective $\text{TiOH}(\text{OSi})_3$ at the T1 crystallographic site in Ti-MWW.^{27,44} Hence, a fraction of Ti atoms, in $\text{Ti-MWW-HNO}_3\text{-calc}$ is tetra-coordinated, probably in a distorted tetrahedral coordination, due to the presence of the hydroxyl ligand.

The spectroscopic characterization suggests that the HNO_3 treatment is almost the only responsible for the Ti insertion in the zeolite framework. This could indicate that the Ti insertion occur when the zeolitic framework is already formed. Looking at the literature data, a reduced amount of interacting Si-OH groups was observed in TS-1 compared to S-1, suggesting a possible healing effect of Ti sites on Si-OH nests.⁸⁸ In $\text{Ti-MWW-HNO}_3\text{-calc}$ this effect is not observed compared with ITQ-1-calc, but this could be due to an effect of the HNO_3 washing on the Si-OH population of $\text{Ti-MWW-HNO}_3\text{-calc}$. Support to the possibility of Ti insertion in defective position in $\text{Ti-MWW-HNO}_3\text{-calc}$ arises from the preferential location of $\text{TiOH}(\text{OSi})_3$ reported to occur at the T1 crystallographic site,²⁷ coupled with the fact that the T1 is surely a Si-OH species during the acid treatment.⁴² Further studies are needed to clarify this point.

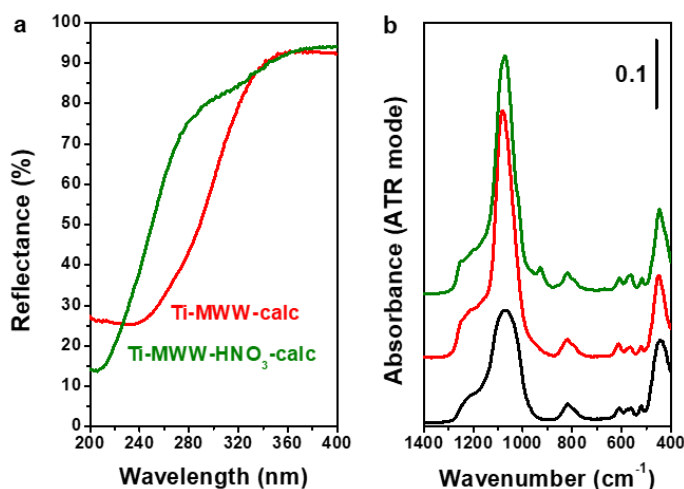


Figure 3. (a) UV-Vis spectra in DR mode of activated samples: Ti-MWW-HNO₃-calc (olive) and Ti-MWW-calc (red). (b) Vertically shifted ATR-IR spectra of activated samples; from top to bottom: Ti-MWW-HNO₃-calc (olive), Ti-MWW-calc (red) and ITQ-1-calc (black).

Study of acid sites and hydroxyls group using probe molecules

The possible acidic sites present in Ti-zeolites generally are (i) the Ti(IV) sites in tetrahedral coordination, acting as Lewis centers and (ii) the hydroxyl groups (Si-OH and Ti-OH), acting as weak Brønsted sites. IR spectroscopy in presence of basic probe molecules is a powerful technique to evaluate the strength and location of these sites, whose study is of fundamental importance for their possible effects on the catalytic activity involving by-products formation.^{4,89} In this work, probe molecules with different protonic affinity, namely CO (Figures S9-S10), CD₃CN (Figure 4), Py (Figure S11-S12) and NH₃ (Figure S13) were employed to study the Ti(IV) Lewis sites of Ti-MWW-HNO₃-calc compared to those of the Ti-free reference ITQ-1-calc and their Si(Ti)-OH population. For the sake of brevity, the detailed description of the spectral properties connected to the adsorption of each probe molecule on the sample surface is reported in the ESI file, while the useful information is reported here. In all the figures, the effect of the maximum coverage is reported in bold (olive and black for Ti-MWW-HNO₃-calc and ITQ-1-calc respectively), while the spectra collected after the progressive outgassing are reported in grey.

Unfortunately, CO (Figure S9-S10) is a poorly informative probe, since its low proton affinity does not allow its interaction with the Ti(IV) Lewis sites when it is in tetrahedral coordination, and the very similar stretching frequency of Si-OH and Ti-OH prevent the discrimination between probe molecules interacting with Ti-OH respect to Si-OH groups.⁴ For this reason, no significant differences are present between the spectra recorded during the experiment of CO adsorbed on Ti-MWW-HNO₃-calc and on ITQ-1-calc (Figures S9-S10).

In contrast, CD₃CN (Figure 4) is a stronger base than CO, allowing the detection of Ti(IV) in tetrahedral coordination in Ti-MWW-HNO₃-calc (Figure 4a, c). Upon CD₃CN dosage, the Si(Ti)-OH---NCCD₃ complex forms, determining the consumption of the bands above 3600 cm⁻¹ (Figure 4a), associated to external, internal and terminal hydroxyls groups, and the parallel formation of a broad band, in the OH stretching region, with apparent maximum at around 3400 cm⁻¹ (Figure 4a).^{71,90} The corresponding spectra of CD₃CN adsorbed on the reference ITQ-1-calc sample exhibit the same behavior in the high frequency region (Figure 4d).

In the CN stretching spectral range (Figure 4b), the bands of physisorbed, H-bonded and interacting with Ti(IV) CD₃CN are present at 2264, 2274 and 2307 cm⁻¹ respectively. The interaction of hydroxyls groups and Ti(IV) sites is reversible at RT, except for the band at 3688 cm⁻¹. However, it is not possible to determine if this band could be ascribed to strong (or medium strength) Brønsted acid sites, since the presence of the band assigned to CN stretching of CD₃CN coordinated on Brønsted acid sites at 2284 cm⁻¹⁹⁰ is not evident. It is worth noting that the spectrum of the reference ITQ-1-calc reports only the components at 2264 and 2274 cm⁻¹ generated by weakly physisorbed and interacting with OH groups CD₃CN respectively (Figure 4e).

The band at 2307 cm^{-1} , observed in the CN stretching ($\nu(\text{CN})$) region of Ti-MWW- HNO_3 -calc, is assigned to CD_3CN in interaction with Ti(IV) Lewis acid sites in tetrahedral coordination. The same band was observed in TS-1 at 2303 cm^{-1} .⁷¹ The shift to higher frequencies ($+43\text{ cm}^{-1}$ compared to the $\nu(\text{CN})$ frequency of weakly physisorbed CD_3CN) testifies the stronger acid character of the Ti(IV) Lewis acid site in Ti-MWW- HNO_3 -calc compared to the same site in TS-1 (shift of $+37\text{ cm}^{-1}$).^{71,88} In comparison, the formation of Al(III)- NCCD_3 adducts in ZSM-5 gives rise to a higher upward shift ($+50\text{ cm}^{-1}$), as expected for a strong Lewis site.⁷¹ It implies that the Ti(IV) sites in Ti-MWW have a medium acid strength. The stronger acidity of Ti(IV) in Ti-MWW is coherent with the presence of $\text{TiOH}(\text{SiO}_3)$ species, indicated as more acidic than the fully coordinated tetrahedral sites.^{64,65} Moreover, this peculiarity helps explaining the interesting catalytic activity in epoxidation reactions already reported for Ti-containing MWW zeolites.^{27,44} Figures 4c and 4f show the spectra of Ti-MWW- HNO_3 -calc and ITQ-1-calc in the framework vibrations region upon CD_3CN dosing and outgassing. In Ti-MWW- HNO_3 -calc, the band at 930 cm^{-1} present on activated sample and typical of Ti-MWW materials upward shifts to 944 cm^{-1} , as similarly occurred to the 960 cm^{-1} band in a similar experiment performed on TS-1 (shift of $+10\text{ cm}^{-1}$).⁷¹ The shift observed for the 944 cm^{-1} band is totally reversible, indeed, after CD_3CN outgassing, it comes back to its original position. In contrast, upon CD_3CN dosage, the band at 965 cm^{-1} , related to the presence of Ti atoms in tetrahedral coordination, increases in intensity and broadens without shifting.

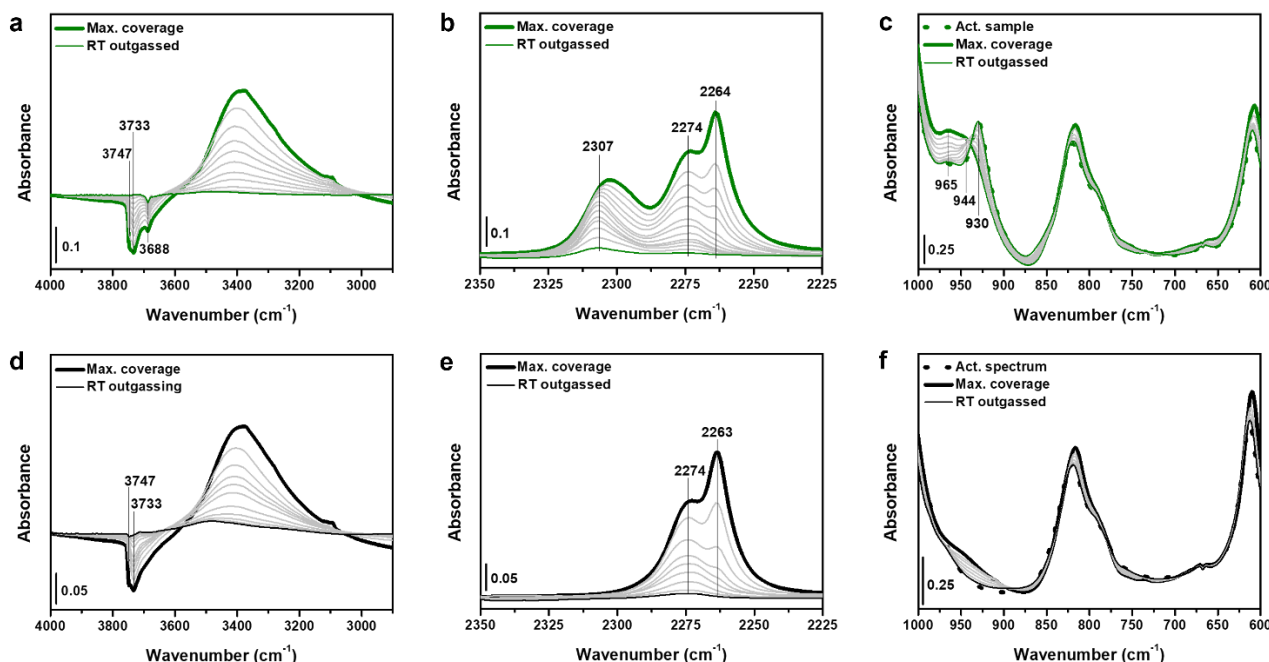


Figure 4. Background subtracted IR spectra of (a, b) Ti-MWW- HNO_3 -calc and (d, e) ITQ-1-calc after contact with CD_3CN at RT, in the (a, d) $4000\text{-}2900\text{ cm}^{-1}$ and (b, e) $2350\text{-}2225\text{ cm}^{-1}$ spectral regions. The spectrum of the sample after outgassing at $500\text{ }^\circ\text{C}$ was used as background. IR spectra of (c) Ti-MWW- HNO_3 -calc and (f) ITQ-1-calc after contact with CD_3CN in the framework vibration region ($1000\text{-}600\text{ cm}^{-1}$).

Figure S11 shows the background subtracted IR spectra of adsorbed Py on Ti-MWW-HNO₃-calc (a, b) and ITQ-1-calc (c, d) in the hydroxyl and ring deformation spectral regions (4000-2600 and 1650-1350 cm⁻¹ respectively). The assignment of the signals related to Py adsorbed on Ti-MWW-HNO₃-calc are summarized in Table S1. Concerning Ti-MWW-HNO₃-calc, the OH groups are partially perturbed by the interaction with Py (Figure S11a). This molecule, despite its wider kinetic diameter (0.57 nm) is still able to enter in the micropores of zeolites with MWW framework, but it cannot interact with a fraction of the hydroxyl groups present in defective sites (nests) (Figure S12). It also interacts with the family of Si(Ti)-OH absorbing at 3688 cm⁻¹, suggesting that they are not located inside the fraction of the smallest nests. The adsorption of Py on the ITQ-1-calc sample (Figure S11c) shows an analogous behavior in the OH stretching spectral range.

The last probe used in this work is the NH₃ (Figure S13), the stronger base usually employed for IR studies. This choice was done to explore the possible presence of medium strength Bronsted acid sites. Actually, the bands at 1477 and 1483 cm⁻¹, in Ti-MWW-HNO₃-calc and ITQ-1-calc respectively, can be detected after NH₃ adsorption and can be tentatively assigned to NH₄⁺ bending modes (usually found in the 1500-1350 cm⁻¹ range).⁹¹⁻⁹³ The signal is present independently of the Ti presence in the framework and, contrarily to the usual signal of protonated NH₄⁺ generated by strong Brønsted acidic sites, it completely disappears upon outgassing at RT. The same spectral behavior was already reported for zeolites free from heteroatoms.^{51,78}

Study of the interaction with H₂O₂

Figure 5 shows the effect of the interaction with H₂O₂ on the optical properties of Ti-MWW-HNO₃-calc. The olive curve in both panels is the spectrum of Ti-MWW-HNO₃-calc in air, without any activation. For this reason, a fraction of H₂O molecules is still present in the sample, causing the broadening of the LMCT electronic transition involving Ti observed comparing the UV-Vis spectrum in air with the activated one (Figure S6b). The spectrum in air of Ti-MWW-HNO₃-calc exhibits a minimum at 225 nm, compared to the corresponding minimum in the spectrum of TS-1 recorded in air, at 220 nm.¹² The higher shift could be due to an increased distortion of the tetrahedral geometry when H₂O molecules expand the coordination sphere of the Ti sites.^{94,95} This is coherent with the presence of TiOH(SiO)₃ sites, whose geometry is less constrained than Ti(OSi)₄ one.

Upon interaction with H₂O₂, a pale orange wet powder is obtained (orange full curves in Figure 5). The baseline in the visible and NIR regions of the spectrum decreased in reflectance due to the presence of liquid H₂O in the interparticle voids, that strongly modifies the scattering profile of the powder (Figure S7). The excess of H₂O can be seen from the intensity of the signals at 1900 and 1400 nm in the NIR region, assigned to combination and overtone modes of H₂O.¹² Drying the powder for 24 h at RT, a significant decrease of the adsorbed H₂O is visible. Simultaneously, the scattering baseline converged to that of the naturally hydrated powder (comparison of ocher/yellow spectra with olive one), except for the inevitable slight difference due

to powder positioning in the sample holder. A longer drying (96 h) does not lead to further modification in the NIR region.

In the orange spectrum, as observed in TS-1,¹² the LMCT band involving Ti shows a broadening due to the water excess and a shoulder around 385 nm, assigned to the LMCT of a “side-on” peroxy ligand to the Ti center (Ti-OO⁻), which confers to the material the typical pale orange color.¹² Upon dehydration, the stable complex, Ti-OOH forms.¹² The degradation of the Ti-OOH/Ti-OO⁻ complexes occurs during the sample dehydration. Indeed, 24 h of drying give rise to an increase of the reflectance at 385 nm from 17% (orange spectrum) to 62% (yellow spectrum); an elapsed drying of 96 h (ocher spectrum) causes a further increase to 73%. Considering what reported¹² for an analogous experiment performed on TS-1, the degradation of the Ti-OOH/Ti-OO⁻ complex seems to occur faster in Ti-MWW than in TS-1, and consequently the complexes appear to be more labile at RT and ambient pressure in Ti-MWW respect to what happens in TS-1. The Ti atoms in TiOH(OSi)₃ species are less constrained and less bound to the framework respect to fully coordinated Ti(OSi)₄ species and consequently the formed complexes are less stable in time. The same powder, wet with H₂O₂ and then dried for 96 h, was put again in contact with H₂O₂ to verify the cyclability of the Ti-OOH/Ti-OO⁻ complexes (dashed spectra in Figure 5b). The process turned out to be fully reversible. The dashed orange and dashed yellow curves show that the Ti-OOH/Ti-OO⁻ complexes are formed again (at a similar level of hydration) and that their degradation occurs again in 24 h.

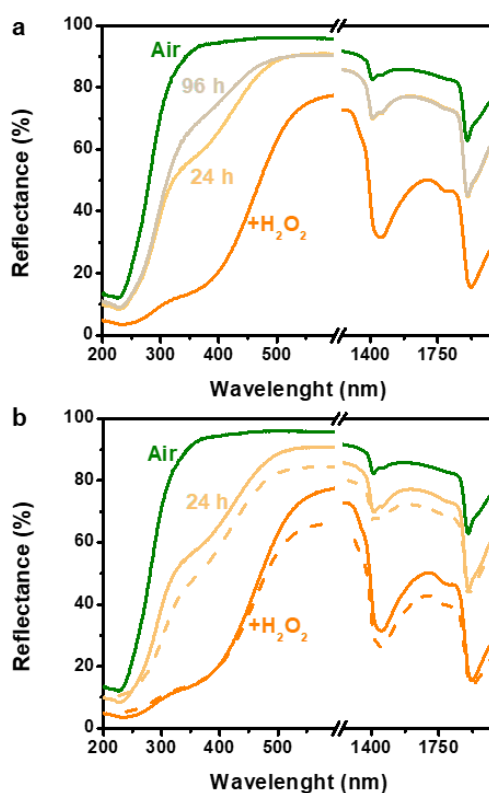


Figure 5. UV-Vis-NIR spectra in DR mode, recorded in different conditions. (a) First contact of Ti-MWW-HNO₃-calc with H₂O₂ (+H₂O₂, full orange), dried for 24 (full yellow) and 96 (full ocher) h, respect to the reference Ti-

MWW-HNO₃-calc as-such in air (full olive). (b) The same as in panel a, compared to the second contact with H₂O₂ (dashed orange) and subsequent drying for 24 h (dashed yellow).

Figure S14 shows the effect of rehydration after H₂O₂ contact and consecutive drying for 4 h (a) or 96 h (b). Water affects the equilibrium $Ti - OOH + nH_2O \rightleftharpoons [Ti - OO]^- + H_3O^+(H_2O)_{n-1}$. In TS-1 the partial regeneration of the Ti-OO⁻ species occurs upon rehydration,¹² without further contact with H₂O₂. The regeneration of Ti-OO⁻ species is also observed in Ti-MWW-HNO₃-calc upon contact with H₂O after 4 h of drying (Figure S14a), as highlighted by the decrease of reflectance at 385 nm. In contrast, the sample dried for 96 h does not exhibit the same behavior (Figure S14b). Visually, upon rehydration of 4 h dried sample, the pale orange powder comes back to bright orange, while it does not occur on the 96 h dried Ti-MWW-HNO₃-calc. Probably, at prolonged drying times, the residual amount of Ti-OOH species is too low to regenerate the Ti-OO⁻ complex.

Finally, the sample contacted twice with H₂O₂ was regenerated by calcination and the Ti speciation were determined by UV-Vis (Figure S14c) and ATR-IR spectroscopies (Figure S14d). The formation of a shoulder at high wavelength in the UV-Vis spectra (dashed light green curve in Figure S14c) and the decrease of the band at 930 cm⁻¹ ascribed to in framework Ti in the ATR-IR spectra (light green spectrum in Figure S14d) suggest that a fraction of Ti has come out of the framework, but that most of the Ti atoms are still located in framework positions.

The H₂O₂ interaction with Ti-MWW-HNO₃-calc was further studied by *in situ* IR spectroscopy (Figure 6a, Figure S15-S17). The use of IR spectroscopy is complicated by the impossibility of dosing H₂O₂ in vapor phase on the pelletized sample, but it has the advantage of observing *in situ* the formation of the reaction products. The experiment was conducted on a pellet soaked with an aqueous H₂O₂ solution (30 wt%). The H₂O₂ and H₂O excesses were rapidly outgassed and, when the H₂O bending mode at 1630 cm⁻¹ disappeared, 40 mbar of gaseous propylene were dosed on the sample. For comparison, spectra recorded during H₂O outgassing on pure Ti-MWW-HNO₃-calc are reported in Figure S15. The difficulty of this experimental procedure lies in the need to remove the larger fraction of molecularly adsorbed H₂O, to avoid overlapping of the intense H₂O signals with the bands related to propylene and propylene oxide (Figure 6b), and, at the same time without leading to the degradation of the Ti-OOH/Ti-OO⁻ complexes, labile in vacuum conditions.⁹⁶

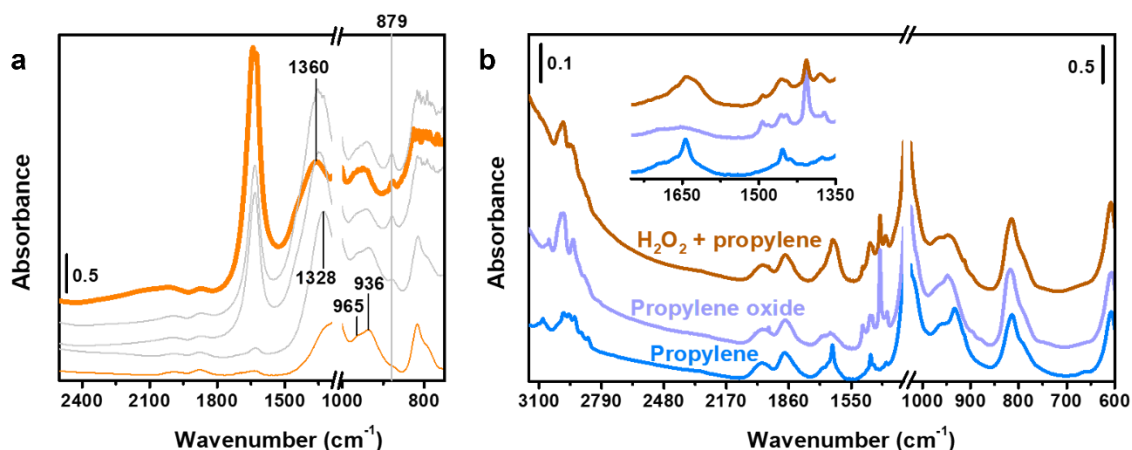


Figure 6. IR spectra in the 2500-750 cm^{-1} spectral range of (a) Ti-MWW- HNO_3 -calc recorded after soaking the pellet with a $\text{H}_2\text{O}_2/\text{H}_2\text{O}$ 30 wt% solution (bold orange), during the outgassing of the $\text{H}_2\text{O}_2/\text{H}_2\text{O}$ excess (top to bottom, grey to orange curves). The spectra are vertically shifted for the sake of clarity. (b) IR spectrum recorded after 5 min from the dosing of 40 mbar of propylene on the H_2O_2 soaked/outgassed sample (dark orange) and on the RT outgassed sample (blue) and after dosing propylene oxide on the RT outgassed sample (light purple); the spectra are vertically shifted for the sake of clarity.

The presence of liquid H_2O_2 on the pellet is visible from the bending vibration of the -OH group of H_2O_2 that shifts from 1360 to 1328 cm^{-1} and decreases in intensity upon removing the excess of H_2O_2 and H_2O .⁹⁶ The stretching mode of O-O group in physisorbed H_2O_2 is observed at 879 cm^{-1} (Figure 6a).⁹⁶ Actually, in TS-1, an analogous signal a is found at 880 cm^{-1} .⁹⁶ The same spectral region should host the O-O stretching modes of Ti-OO^- and Ti-OOH complexes, but they can be hardly observed at RT. In TS-1, they were observed at -43 $^\circ\text{C}$ respectively at 836 and 886 cm^{-1} .⁹⁶ The complexation of Ti(IV) sites by H_2O_2 in Ti-MWW was proved by dosing CD_3CN on the H_2O_2 soaked and RT rapidly outgassed sample (Figure S17). The spectra from bold to thin orange (Figure S17a) are analogous to those in Figure 6a and the spectra from bold to thin olive are due to CD_3CN interaction with the sample after saturating Ti(IV) sites with H_2O_2 aqueous solution. Figure S17b shows the CN stretching vibration region of bold to thin olive curves, upon progressive outgassing (analogous to Figure 4b). Here, the bands of physisorbed CD_3CN (at 2264 cm^{-1}) and H-bonded CD_3CN (at 2274 cm^{-1}), probably due to the interaction of CD_3CN with adsorbed H_2O molecules are present. The signal at 2307 cm^{-1} assigned to CD_3CN in interaction with the Ti(IV) Lewis sites is less intense compared to the experiment performed without H_2O_2 (Figure S17c). This confirms that upon interaction with H_2O_2 aqueous solution the saturation of most of the Ti(IV) Lewis sites occurs.

When propylene was dosed on H_2O_2 soaked and rapidly outgassed Ti-MWW- HNO_3 -calc (Figure 6b and S16), the formation of propylene oxide was almost immediate (dark orange curve in Figure 6b). The rate of the reaction prevents the observation of any kind of intermediate species and of the propylene adsorbed over the H_2O_2 soaked pellet (Figure S16). The more prominent vibrational modes of propylene can be observed in

the blue curve (Figures 6b and S16), obtained upon dosing propylene on Ti-MWW-HNO₃-calc without H₂O₂/H₂O contact. The bands assigned to CH₃ asymmetric and symmetric deformation fall at 1453 cm⁻¹ and 1375 cm⁻¹ respectively⁹⁷ and the band ascribed to C=C stretching mode is found at 1643 cm⁻¹.⁹⁷ The more prominent bands due to the presence of propylene oxide (light purple curve in Figures 6b and S16) are instead the bands at 1371 cm⁻¹ (CH₃ symmetric deformation), 1407 cm⁻¹ (with a combined character of CH₃ symmetric deformation and C-H in-plane bending),^{97,98} 1445 and 1456 cm⁻¹ (assigned to CH₃ asymmetric deformation with different symmetries) and 1493 cm⁻¹ (assigned to CH₂ bending mode).^{97,98} The out-of-scale Si-O-Si stretching vibration completely covers the breathing mode of the epoxide ring (in the 1290-1235 cm⁻¹ range).^{97,98} The orange curve shows prevalently the signals of propylene oxide, testifying that Ti-MWW-HNO₃-calc is active in the propylene epoxidation.

Conclusions

In this work, the synthesis of Ti-MWW was reproduced from the literature and high Ti loadings, were reached (1.7 wt% of TiO₂), almost entirely in tetrahedral coordination. On the synthetic side, the effect of the HNO₃ post-treatment washing was investigated. The oxidant properties of HNO₃ helped in the OSDA removal, starting its elimination already during the acid treatment. Moreover, the acidic conditions cause the removal of any K residuals from the framework. This is extremely important, since the presence of alkaline metals is detrimental to the Ti insertion in the tetrahedral positions of the framework. By analysing the ATR-IR and the UV spectra of the washed (Ti-MWW-HNO₃-calc) and not washed (Ti-MWW-calc) samples, the HNO₃ treatment was demonstrated to be the only responsible for the Ti insertion in the framework.

On the spectroscopic side, the use of IR spectroscopy and targeted probe molecules allows determining that the Lewis acid sites embodied by the uncoordinated Ti tetrahedral sites are stronger than the corresponding ones in TS-1. This is due to the massive presence of acidic TiOH(SiO)₃ sites in the Ti-MWW.

The interaction of the Ti sites of Ti-MWW with H₂O₂ was studied by IR and UV-Vis spectroscopies. The Ti-OO⁻ and Ti-OOH complexes appears to be more labile than in TS-1, as their degradation at RT and under ambient pressure seems faster than in TS-1. This study proved that after two cycles of contacts with H₂O₂ and consequent drying, the Ti-MWW-HNO₃-calc sample was regenerated by simple calcination. The regeneration step was accompanied by only a slight leaching of tetrahedral Ti species. However, the regeneration and stability of the Ti species in reaction conditions, such as in methanol/H₂O₂ solution (often used in reactions instead of H₂O medium) deserve to be explored further.^{99,100} Despite the differences in the stability of the complexes and the differences in the Ti sites acidity, the Ti-MWW-HNO₃-calc sample is demonstrated to be active in the epoxidation of propylene, as the TS-1 catalyst is.

Acknowledgments

The authors acknowledge support from the Project CH4.0 under the MUR program "Dipartimenti di Eccellenza 2023-2027" (CUP: D13C22003520001). The authors acknowledge Prof. Mery Malandrino and Dr. Maria Carmen Valsania for elemental analysis (ICP-OES and SEM-EDX respectively) and for fruitful discussion.

References

- (1) Smeets, V.; Gaigneaux, E. M.; Debecker, D. P. Titanosilicate Epoxidation Catalysts: A Review of Challenges and Opportunities. *ChemCatChem* **2022**, *14* (1), e202101132. <https://doi.org/10.1002/cctc.202101132>.
- (2) Nie, X.; Ji, X.; Chen, Y.; Guo, X.; Song, C. Mechanistic Investigation of Propylene Epoxidation with H₂O₂ over TS-1: Active Site Formation, Intermediate Identification, and Oxygen Transfer Pathway. *Mol. Catal.* **2017**, *441*, 150–167. <https://doi.org/10.1016/j.mcat.2017.08.011>.
- (3) Clerici, M. G.; Ingallina, P. Epoxidation of Lower Olefins with Hydrogen Peroxide and Titanium Silicalite. *J. Catal.* **1993**, *140*, 71–83.
- (4) Signorile, M.; Crocellà, V.; Damin, A.; Rossi, B.; Lamberti, C.; Bonino, F.; Bordiga, S. Effect of Ti Speciation on Catalytic Performance of TS-1 in the Hydrogen Peroxide to Propylene Oxide Reaction. *J. Phys. Chem. C* **2018**, *122* (16), 9021–9034. <https://doi.org/10.1021/acs.jpcc.8b01401>.
- (5) Yin, J.; Xu, H.; Wang, B.; Tian, W.; Yin, J.; Jiang, J.; Wu, P. Highly Selective 1-Pentene Epoxidation over Ti-MWW with Modified Microenvironment of Ti Active Sites. *Catal. Sci. Technol.* **2020**, *10* (17), 6050–6064. <https://doi.org/10.1039/d0cy00478b>.
- (6) Shima, H.; Tatsumi, T.; Kondo, J. N. Direct FT-IR Observation of Oxidation of 1-Hexene and Cyclohexene with H₂O₂ over TS-1. *Microporous Mesoporous Mater.* **2010**, *135* (1–3), 13–20. <https://doi.org/10.1016/j.micromeso.2010.06.005>.
- (7) Wróblewska, A. Water as the Solvent for the Process of Phenol Hydroxylation over the Ti-MWW Catalyst. *React. Kinet. Mec. Catal.* **2013**, *108* (2), 491–505. <https://doi.org/10.1007/s11144-012-0517-2>.
- (8) Klaewkla, R.; Kulprathipanja, S.; Rangsunvigit, P.; Rirksomboon, T.; Nemeth, L. Phenol Hydroxylation Using Ti- and Sn-Containing Silicalites. *Chem. Commun.* **2003**, *3* (13), 1500–1501. <https://doi.org/10.1039/b303455k>.
- (9) Esposito, A.; Taramasso, M.; Neri, C. Hydroxylating Aromatic Hydrocarbons. US Patent 4396783, 1983.
- (10) Liu, H.; Lu, G.; Guo, Y.; Guo, Y. Synthesis of TS-1 Using Amorphous SiO₂ and Its Catalytic Properties for Hydroxylation of Phenol in Fixed-Bed Reactor. *Appl. Catal. A Gen.* **2005**, *293* (1–2), 153–161. <https://doi.org/10.1016/j.apcata.2005.07.021>.
- (11) Bellussi, G.; Millini, R. Background and Recent Advances in Ti-Containing Zeolite Materials. **2017**, 1–52. https://doi.org/10.1007/430_2017_15.
- (12) Bonino, F.; Damin, A.; Ricchiardi, G.; Ricci, M.; Spanò, G.; D'Aloisio, R.; Zecchina, A.; Lamberti, C.; Prestipino, C.; Bordiga, S. Ti-Peroxo Species in the TS-1/H₂O₂/H₂O System. *J. Phys. Chem. B* **2004**, *108* (11), 3573–3583. <https://doi.org/10.1021/jp036166e>.

- (13) Taramasso, M.; Perego, G.; Notari, B. Preparation of Porous Crystalline Synthetic Material Comprised of Silicon and Titanium Oxides. US Patent 4410501, 1983.
<https://patents.google.com/patent/US4410501A/en>.
- (14) Pena, M. L.; Dellarocca, V.; Rey, F.; Corma, A.; Coluccia, S.; Marchese, L. Elucidating the Local Environment of Ti(IV) Active Sites in Ti-MCM-48: A Comparison between Silylated and Calcined Catalysts. *Microporous Mesoporous Mater.* **2001**, *44*, 345–356.
- (15) Bai, R.; Song, Y.; Bai, R.; Yu, J. Creation of Hierarchical Titanosilicate TS-1 Zeolites. *Adv. Mater. Interfaces* **2021**, *8*, 2001095.
- (16) Wu, Z.; Wang, B.; Shi, J.; Rui, P.; Xie, X.; Liao, W.; Shu, X. The Silanization Process for the Hydrothermal Synthesis of Hierarchical Titanium Silicalite-1. *Microporous Mesoporous Mater.* **2021**, *327*, 111407.
<https://doi.org/10.1016/j.micromeso.2021.111407>.
- (17) Zhang, J.; Jin, S.; Deng, D.; Liu, W.; Tao, G.; Luo, Q.; Sun, H.; Yang, W. Insight into the Formation of Framework Titanium Species during Acid Treatment of MWW-Type Titanosilicate and the Effect of Framework Titanium State on Olefin Epoxidation. *Microporous Mesoporous Mater.* **2021**, *314*.
<https://doi.org/10.1016/j.micromeso.2020.110862>.
- (18) Smeets, V.; Gaigneaux, E. M.; Debecker, D. P. Hierarchical Micro-/Macroporous TS-1 Zeolite Epoxidation Catalyst Prepared by Steam Assisted Crystallization. *Microporous Mesoporous Mater.* **2020**, *293*, 109801. <https://doi.org/10.1016/j.micromeso.2019.109801>.
- (19) Kong, Z.; Yue, B.; Deng, W.; Zhu, K.; Yan, M.; Peng, Y.; He, H. Direct Synthesis of Hierarchically Porous TS-1 through a Solvent-Evaporation Route and Its Application as an Oxidation Catalyst. *Appl. Organomet. Chem.* **2014**, *28* (4), 239–243. <https://doi.org/10.1002/aoc.3115>.
- (20) Blasco, T.; Cambor, M. A.; Corma, A.; Esteve, P.; Guil, J. M.; Martínez, A.; Perdigón-Melón, J. A.; Valencia, S. Direct Synthesis and Characterization of Hydrophobic Aluminum-Free Ti-Beta Zeolite. *J. Phys. Chem. B* **1998**, *102*, 75–88.
- (21) Wilkenhöner, U.; Gammon, D. W.; Steen, E. Van. Intrinsic Activity of Titanium Sites in TS-1 and Al-Free Ti-Beta. *Stud. Surf. Sci. Catal.* **2002**, *142 A*, 619–626. [https://doi.org/10.1016/S0167-2991\(02\)80081-7](https://doi.org/10.1016/S0167-2991(02)80081-7).
- (22) Blasco, T.; Corma, A.; Navarro, T.; Pariente, J. P. Synthesis, Characterization, and Catalytic Activity of Ti-MCM-41 Structures. *J. Catal.* **1995**, *156*, 65–74.
- (23) Corma, A.; Kan, Q.; Rey, F. Synthesis of Si and Ti Si-MCM-48 Mesoporous Materials with Controlled Pore Sizes in the Absence of Polar Organic Additives and Alkali Metal Ions. *Chem. Commun.* **1998**, 579–580.
- (24) Damin, A.; Bordiga, S.; Zecchina, A.; Doll, K.; Lamberti, C. Ti-Chabazite as a Model System of Ti(IV) in Ti-Zeolites: A Periodic Approach. *J. Chem. Phys.* **2003**, *118* (22), 10183–10194.
<https://doi.org/10.1063/1.1571516>.
- (25) Díaz-Cabañas, M. J.; Villaescusa, L. A.; Cambor, M. A. Synthesis and Catalytic Activity of Ti-ITQ-7: A New Oxidation Catalyst with a Three-Dimensional System of Large Pore Channels. *Chem. Commun.* **2000**, No. 9, 761–762. <https://doi.org/10.1039/b000539h>.
- (26) Wu, P.; Tatsumi, T. Preparation of B-Free Ti-MWW through Reversible Structural Conversion. *Chem. Commun.* **2002**, *2* (10), 1026–1027. <https://doi.org/10.1039/b201170k>.

- (27) Xu, H.; Guan, Y.; Lu, X.; Yin, J.; Li, X.; Zhou, D.; Wu, P. Relation of Selective Oxidation Catalytic Performance to Microenvironment of Ti^{IV} Active Site Based on Isotopic Labeling. *ACS Catal.* **2020**, *10* (8), 4813–4819. <https://doi.org/10.1021/acscatal.0c00439>.
- (28) Waal, J. C. Van Der; Bekkum, H. Van. Zeolite Titanium Beta: A Versatile Epoxidation Catalyst. Solvent Effects. *J. Mol. Catal. A Chem.* **1997**, *124*, 137–146.
- (29) Hulea, V.; Dumitriu, E.; Patcas, F.; Ropot, R.; Grafn, P.; Moreau, P. Cyclopentene Oxidation with H₂O₂ over Ti-Containing Zeolites. *Appl. Catal. A Gen.* **1998**, *170*, 169–175.
- (30) Kwon, O.; Ayla, E. Z.; Potts, D. S.; Flaherty, D. W. Effects of Solvent-Pore Interaction on Rates and Barriers for Vapor Phase Alkene Epoxidation with Gaseous H₂O₂ in Ti-BEA Catalysts. *ACS Catal.* **2023**, *13* (9), 6430–6444. <https://doi.org/10.1021/acscatal.3c00730>.
- (31) Rosso, F.; Rizzetto, A.; Airi, A.; Khoma, K.; Signorile, M.; Crocellà, V.; Bordiga, S.; Galliano, S.; Barolo, C.; Alladio, E.; Bonino, F. Rationalization of TS-1 Synthesis through the Design of Experiments. *Inorg. Chem. Front.* **2022**, *9* (14). <https://doi.org/10.1039/d2qi00643j>.
- (32) Ahn, W. S.; Lee, D. H.; Kim, T. J.; Kim, J. H.; Seo, G.; Ryoo, R. Post-Synthetic Preparations of Titanium-Containing Mesopore Molecular Sieves. *Appl. Catal. A Gen.* **1999**, *181*, 39–49.
- (33) Zhang, S.; Jin, S.; Tao, G.; Wang, Z.; Liu, W.; Chen, Y.; Luo, J.; Zhang, B.; Sun, H.; Wang, Y.; Yang, W. The Evolution of Titanium Species in Boron-Containing Ti-MWW Zeolite during Post-Treatment Revealed by UV Resonance Raman Spectroscopy. *Microporous Mesoporous Mater.* **2017**, *253*, 183–190. <https://doi.org/10.1016/j.micromeso.2017.07.006>.
- (34) Su, J.; Xiong, G.; Zhou, J.; Liu, W.; Zhou, D.; Wang, G.; Wang, X.; Guo, H. Amorphous Ti Species in Titanium Silicalite-1: Structural Features, Chemical Properties, and Inactivation with Sulfosalt. *J. Catal.* **2012**, *288*, 1–7. <https://doi.org/10.1016/j.jcat.2011.12.006>.
- (35) Zuo, Y.; Liu, M.; Zhang, T.; Hong, L.; Guo, X.; Song, C.; Chen, Y.; Zhu, P.; Jaye, C.; Fischer, D. Role of Pentahedrally Coordinated Titanium in Titanium Silicalite-1 in Propene Epoxidation. *RSC Adv.* **2015**, *5* (23), 17897–17904. <https://doi.org/10.1039/c5ra00194c>.
- (36) Liu, Y.; Wang, F.; Zhang, X.; Zhang, Q.; Zhai, Y.; Lv, G.; Li, M.; Li, M. One-Step Synthesis of Anatase-Free Hollow Titanium Silicalite-1 by the Solid-Phase Conversion Method. *Microporous Mesoporous Mater.* **2022**, *331*, 111676. <https://doi.org/10.1016/j.micromeso.2021.111676>.
- (37) Li, M.; Zhai, Y.; Zhang, X.; Wang, F.; Lv, G.; Rosine, A.; Li, M.; Zhang, Q.; Liu, Y. (NH₄)₂SO₄-Assisted Synthesis of Thin-Walled Ti-Rich Hollow Titanium Silicalite-1 Zeolite for 1-Hexene Epoxidation. *Microporous Mesoporous Mater.* **2022**, *331*, 111655. <https://doi.org/10.1016/j.micromeso.2021.111655>.
- (38) Lucas, A. De; Rodríguez, L.; Sánchez, P. Optimization of the Molar Composition of the Gel in the Synthesis of Titanium Silicalite TS-2. *Chem. Eng. Res. Des.* **2000**, *78* (1), 136–144. <https://doi.org/10.1205/026387600526979>.
- (39) Eilertsen, E. A.; Bordiga, S.; Lamberti, C.; Damin, A.; Bonino, F.; Arstad, B.; Svelle, S.; Olsbye, U.; Lillerud, K. P. Synthesis of Titanium Chabazite: A New Shape Selective Oxidation Catalyst with Small Pore Openings and Application in the Production of Methyl Formate from Methanol. *ChemCatChem* **2011**, *3* (12), 1869–1871. <https://doi.org/10.1002/cctc.201100281>.

- (40) Pitinova-Stekrova, M.; Eliášová, P.; Weissenberger, T.; Shamzhy, M.; Musilová, Z.; Čejka, J. Highly Selective Synthesis of Campholenic Aldehyde over Ti-MWW Catalysts by α -Pinene Oxide Isomerization. *Catal. Sci. Technol.* **2018**, *8* (18), 4690–4701. <https://doi.org/10.1039/c8cy01231h>.
- (41) Leonowicz, M. E.; Lawton, J. A.; Lawton, S. L.; Rubin, M. K. MCM-22: A Molecular Sieve with Two Independent Multidimensional Channel Systems. *Science (1979)* **1994**, *264* (5167), 1910–1913. <https://doi.org/10.1126/science.264.5167.1910>.
- (42) Millini, R.; Perego, G.; Parker, W. O.; Bellussi, G.; Carluccio, L. Layered Structure of ERB-1 Microporous Borosilicate Precursor and Its Intercalation Properties towards Polar Molecules. *Microporous Mater.* **1995**, *4* (2–3), 221–230. [https://doi.org/10.1016/0927-6513\(95\)00013-Y](https://doi.org/10.1016/0927-6513(95)00013-Y).
- (43) Ostroumova, V. A.; Maksimov, A. L. MWW-Type Zeolites: MCM-22, MCM-36, MCM-49, and MCM-56 (A Review). *Petrol. Chem.* **2019**, *59* (8), 788–801. <https://doi.org/10.1134/S0965544119080140>.
- (44) Wu, P.; Tatsumi, T.; Komatsu, T.; Yashima, T. A Novel Titanosilicate with MWW Structure. I. Hydrothermal Synthesis, Elimination of Extraframework Titanium, and Characterizations. *J. Phys. Chem. B* **2001**, *105* (15), 2897–2905. <https://doi.org/10.1021/jp002816s>.
- (45) Položij, M.; Thang, H. V.; Rubeš, M.; Eliášová, P.; Čejka, J.; Nachtigall, P. Theoretical Investigation of Layered Zeolites with MWW Topology: MCM-22P vs. MCM-56. *Dalton Trans.* **2014**, *43* (27), 10443–10450. <https://doi.org/10.1039/c4dt00414k>.
- (46) Tang, Z.; Yu, Y.; Liu, W.; Chen, Z.; Wang, R.; Liu, H.; Wu, H.; Liu, Y.; He, M. Deboronation-Assisted Construction of Defective Ti(OSi)₃OH Species in MWW-Type Titanosilicate and Their Enhanced Catalytic Performance. *Catal. Sci. Technol.* **2020**, *10* (9), 2905–2915. <https://doi.org/10.1039/d0cy00126k>.
- (47) Signorile, M.; Braglia, L.; Crocellà, V.; Torelli, P.; Groppo, E.; Ricchiardi, G.; Bordiga, S.; Bonino, F. Titanium Defective Sites in TS-1: Structural Insights by Combining Spectroscopy and Simulation. *Angew. Chem. Int. Ed.* **2020**, *59* (41), 18145–18150. <https://doi.org/10.1002/anie.202005841>.
- (48) Bordiga, S.; Damin, A.; Bonino, F.; Ricchiardi, G.; Zecchina, A.; Tagliapietra, R.; Lamberti, C. Resonance Raman Effects in TS-1: The Structure of Ti(IV) Species and Reactivity towards H₂O, NH₃ and H₂O₂: An in Situ Study. *Phys. Chem. Chem. Phys.* **2003**, *5* (20), 4390–4393. <https://doi.org/10.1039/b306041c>.
- (49) Bolis, V.; Bordiga, S.; Lamberti, C.; Zecchina, A.; Carati, A.; Rivetti, F.; Spanò, G.; Petrini, G. A Calorimetric, IR, XANES and EXAFS Study of the Adsorption of NH₃ on Ti-Silicalite as a Function of the Sample Pre-Treatment. *Microporous Mesoporous Mater.* **1999**, *30* (1), 67–76. [https://doi.org/10.1016/S1387-1811\(99\)00016-5](https://doi.org/10.1016/S1387-1811(99)00016-5).
- (50) Dong, J.; Zhu, H.; Xiang, Y.; Wang, Y.; An, P.; Gong, Y.; Liang, Y.; Qiu, L.; Zheng, A.; Peng, X.; Lin, M.; Xu, G.; Guo, Z.; Chen, D. Toward a Unified Identification of Ti Location in the MFI Framework of High-Ti-Loaded TS-1: Combined EXAFS, XANES, and DFT Study. *J. Phys. Chem. C* **2016**, *120* (36), 20114–20124. <https://doi.org/10.1021/acs.jpcc.6b05087>.
- (51) Astorino, E.; Peri, J. B.; Willey, R. J.; Busca, G. Spectroscopic Characterization of Silicalite-1 and Titanium Silicalite-1. *J. Catal.* **1995**, *157*, 482–500.
- (52) Gallo, E.; Bonino, F.; Swarbrick, J. C.; Petrenko, T.; Piovano, A.; Bordiga, S.; Gianolio, D.; Groppo, E.; Neese, F.; Lamberti, C.; Glatzel, P. Preference towards Five-Coordination in Ti Silicalite-1 upon Molecular Adsorption. *ChemPhysChem* **2013**, *14* (1), 79–83. <https://doi.org/10.1002/cphc.201200893>.

- (53) Ricchiardi, G.; Damin, A.; Bordiga, S.; Lamberti, C.; Spanò, G.; Rivetti, F.; Zecchina, A. Vibrational Structure of Titanium Silicate Catalysts. A Spectroscopic and Theoretical Study. *J. Am. Chem. Soc.* **2001**, *123* (46), 11409–11419. <https://doi.org/10.1021/ja010607v>.
- (54) Lamberti, C.; Bordiga, S.; Zecchina, A.; Carati, A.; Fitch, A. N.; Artioli, G.; Petrini, G.; Salvalaggio, M.; Marra, G. L. Structural Characterization of Ti-Silicalite-1: A Synchrotron Radiation X-Ray Powder Diffraction Study. *J. Catal.* **1999**, *183* (2), 222–231. <https://doi.org/10.1006/jcat.1999.2403>.
- (55) Henry, P. F.; Weller, M. T.; Wilson, C. C. Structural Investigation of TS-1: Determination of the True Nonrandom Titanium Framework Substitution and Silicon Vacancy Distribution from Powder Neutron Diffraction Studies Using Isotopes. *J. Phys. Chem. B* **2001**, *105* (31), 7452–7458. <https://doi.org/10.1021/jp0107715>.
- (56) Hajar, C. A.; Jacubinas, R. M.; Eckert, J.; Henson, N. J.; Hay, P. J.; Ott, K. C. The Siting of Ti in TS-1 Is Non-Random. Powder Neutron Diffraction Studies and Theoretical Calculations of TS-1 and FeS-1. *J. Phys. Chem. B* **2000**, *104* (51), 12157–12164. <https://doi.org/10.1021/jp002167k>.
- (57) Signorile, M.; Damin, A.; Bonino, F.; Crocellà, V.; Ricchiardi, G.; Lamberti, C.; Bordiga, S. Computational Assessment of Relative Sites Stabilities and Site-Specific Adsorptive Properties of Titanium Silicalite-1. *J. Phys. Chem. C* **2018**, *122* (3), 1612–1621. <https://doi.org/10.1021/acs.jpcc.7b10104>.
- (58) Gale, J. D. A Periodic Density Functional Study of the Location of Titanium within TS-1. *Solid State Sci.* **2006**, *8* (3-4 SPEC. ISS.), 234–240. <https://doi.org/10.1016/j.solidstatesciences.2006.02.011>.
- (59) Njo, S. L.; Koningsveld, H. Van; Graaf, B. Van De. A Combination of the Monte Carlo Method and Molecular Mechanics Calculations: A Novel Way to Study the Ti(IV) Distribution in Titanium Silicalite-1. *J. Phys. Chem. B* **1997**, *101* (48), 10065–10068. <https://doi.org/10.1021/jp971451h>.
- (60) Zhou, D.; Zhang, H.; Zhang, J.; Sun, X.; Li, H.; He, N.; Zhang, W. Density Functional Theory Investigations into the Structure and Spectroscopic Properties of the Ti⁴⁺ Species in Ti-MWW Zeolite. *Microporous Mesoporous Mater.* **2014**, *195*, 216–226. <https://doi.org/10.1016/j.micromeso.2014.04.037>.
- (61) Přeč, J. Catalytic Performance of Advanced Titanosilicate Selective Oxidation Catalysts – a Review. *Catal. Rev. Sci. Eng.* **2018**, *60* (1), 71–131. <https://doi.org/10.1080/01614940.2017.1389111>.
- (62) Tatsumi, T.; Nakamura, M.; Negishi, S.; o. Tominaga, H. Shape-Selective Oxidation of Alkanes with H₂O₂ Catalysed by Titanosilicate. *J. Chem. Soc. Chem. Commun.* **1990**, *202* (6), 476–477. <https://doi.org/10.1039/C39900000476>.
- (63) Wells, D. H.; Delgass, W. N.; Thomson, K. T. Evidence of Defect-Promoted Reactivity for Epoxidation of Propylene in Titanosilicate (TS-1) Catalysts: A DFT Study. *J. Am. Chem. Soc.* **2004**, *126* (9), 2956–2962. <https://doi.org/10.1021/ja037741v>.
- (64) Wu, L.; Tang, Z.; Yu, Y.; Yao, X.; Liu, W.; Li, L.; Yan, B.; Liu, Y.; He, M. Facile Synthesis of a High-Performance Titanosilicate Catalyst with Controllable Defective Ti(OSi)₃OH Sites. *Chem. Commun.* **2018**, *54* (49), 6384–6387. <https://doi.org/10.1039/c8cc02794c>.
- (65) Yu, Y.; Tang, Z.; Wang, J.; Wang, R.; Chen, Z.; Liu, H.; Shen, K.; Huang, X.; Liu, Y.; He, M. Insights into the Efficiency of Hydrogen Peroxide Utilization over Titanosilicate/H₂O₂ Systems. *J. Catal.* **2020**, *381*, 96–107. <https://doi.org/10.1016/j.jcat.2019.09.045>.
- (66) Cambor, M. A.; Corma, A.; Díaz-Cabañas, M. J.; Baerlocher, C. Synthesis and Structural Characterization of MWW Type Zeolite ITQ-1, the Pure Silica Analog of MCM-22 and SSZ-25. *J. Phys. Chem. B* **1998**, *102* (1), 44–51. <https://doi.org/10.1021/jp972319k>.

- (67) Thommes, M.; Kaneko, K.; Neimark, A. V.; Olivier, J. P.; Rodriguez-Reinoso, F.; Rouquerol, J.; Sing, K. S. W. Physisorption of Gases, with Special Reference to the Evaluation of Surface Area and Pore Size Distribution (IUPAC Technical Report). *Pure Appl. Chem.* **2015**, *87* (9–10), 1051–1069. <https://doi.org/10.1515/pac-2014-1117>.
- (68) Corporation, M. I. Microactive. 2012.
- (69) Bordiga, S.; Roggero, I.; Ugliengo, P.; Zecchina, A.; Bolis, V.; Artioli, G.; Buzzoni, R.; Marra, G.; Rivetti, F.; Spano, G.; Lamberti, C. Characterisation of Defective Silicalites. *J. Chem. Soc. Dalton Trans.* **2000**, *21*, 3921–3929. <https://doi.org/10.1039/b004794p>.
- (70) Zecchina, A.; Bordiga, S.; Spoto, G.; Marchese, L.; Petrini, G.; Leofanti, G.; Padovan, M. Silicalite Characterization. 1. Structure, Adsorptive Capacity, and IR Spectroscopy of the Framework and Hydroxyl Modes. *J. Phys. Chem.* **1992**, *96* (12), 4985–4990. <https://doi.org/10.1021/j100191a047>.
- (71) Bonino, F.; Damin, A.; Bordiga, S.; Lamberti, C.; Zecchina, A. Interaction of CD₃CN and Pyridine with the Ti(IV) Centers of TS-1 Catalysts: A Spectroscopic and Computational Study. *Langmuir* **2003**, *19* (6), 2155–2161. <https://doi.org/10.1021/la0262194>.
- (72) Tempelman, C. H. L.; Portilla, M. T.; Martínez-Armero, M. E.; Mezari, B.; Caluwé, N. G. R. De; Martínez, C.; Hensen, E. J. M. One-Pot Synthesis of Nano-Crystalline MCM-22. *Microporous Mesoporous Mater.* **2016**, *220*, 28–38. <https://doi.org/10.1016/j.micromeso.2015.08.018>.
- (73) Fabbiani, M.; Morsli, A.; Confalonieri, G.; Cacciaguerra, T.; Fajula, F.; Haines, J.; Bengueddach, A.; Arletti, R.; Renzo, F. Di. On the Chemical Condensation of the Layers of Zeolite Precursor MCM-22(P). *Microporous Mesoporous Mater.* **2022**, *332*, 111678–111685. <https://doi.org/10.1016/j.micromeso.2021.111678>.
- (74) Bordiga, S.; Ugliengo, P.; Damin, A.; Lamberti, C.; Spoto, G.; Zecchina, A.; Spanò, G.; Buzzoni, R.; Dalloro, L.; Rivetti, F. Hydroxyls Nests in Defective Silicalites and Strained Structures Derived upon Dehydroxylation: Vibrational Properties and Theoretical Modelling. *Top. Catal.* **2001**, *15* (1), 43–52. <https://doi.org/10.1023/A:1009019829376>.
- (75) Pascale, F.; Ugliengo, P.; Civalleri, B.; Orlando, R.; D'Arco, P.; Dovesi, R. Hydrogarnet Defect in Chabazite and Sodalite Zeolites: A Periodic Hartree-Fock and B3-LYP Study. *J. Chem. Phys.* **2002**, *117* (11), 5337–5346. <https://doi.org/10.1063/1.1499477>.
- (76) Medeiros-Costa, I. C.; Dib, E.; Nesterenko, N.; Dath, J. P.; Gilson, J. P.; Mintova, S. Silanol Defect Engineering and Healing in Zeolites: Opportunities to Fine-Tune Their Properties and Performances. *Chem. Soc. Rev.* **2021**, *50* (19), 11156–11179. <https://doi.org/10.1039/d1cs00395j>.
- (77) Dubray, F.; Dib, E.; Medeiros-Costa, I.; Aquino, C.; Minoux, D.; van Daele, S.; Nesterenko, N.; Gilson, J. P.; Mintova, S. The Challenge of Silanol Species Characterization in Zeolites. *Inorg. Chem. Front.* **2022**, *9* (6), 1125–1133. <https://doi.org/10.1039/d1qi01483h>.
- (78) Gianotti, E.; Dellarocca, V.; Marchese, L.; Martra, G.; Coluccia, S.; Maschmeyer, T. NH₃ Adsorption on MCM-41 and Ti-Grafted MCM-41. FTIR, DR UV-Vis-NIR and Photoluminescence Studies. *Phys. Chem. Chem. Phys.* **2002**, *4* (24), 6109–6115. <https://doi.org/10.1039/b207231a>.
- (79) Bellussi, G.; Carati, A.; Clerici, M. G.; Maddinelli, G.; Millini, R. Reactions of Titanium Silicalite with Protic Molecules and Hydrogen Peroxide. *J. Catal.* **1992**, *133* (1), 220–230. [https://doi.org/10.1016/0021-9517\(92\)90199-R](https://doi.org/10.1016/0021-9517(92)90199-R).

- (80) Millini, R.; Massara, E. P.; Perego, G.; Bellussi, G. Framework Composition of Titanium Silicalite-1. *J. Catal.* **1992**, *137* (2), 497–503. [https://doi.org/10.1016/0021-9517\(92\)90176-l](https://doi.org/10.1016/0021-9517(92)90176-l).
- (81) Lin, D.; Zhang, Q.; Qin, Z.; Li, Q.; Feng, X.; Song, Z.; Cai, Z.; Liu, Y.; Chen, X.; Chen, D.; Mintova, S.; Yang, C. Reversing Titanium Oligomer Formation towards High-Efficiency and Green Synthesis of Titanium-Containing Molecular Sieves. *Angew. Chem. Int. Ed.* **2021**, *60* (7), 3443–3448. <https://doi.org/10.1002/anie.202011821>.
- (82) Thangaraj, A.; Eapen, M. J.; Sivasanker, S.; Ratnasamy, P. Studies on the Synthesis of Titanium Silicalite, TS-1. *Zeolites* **1992**, *12*, 943–950.
- (83) Xing, J.; Yuan, D.; Liu, H.; Tong, Y.; Xu, Y.; Liu, Z. Synthesis of TS-1 Zeolites from a Polymer Containing Titanium and Silicon. *J. Mater. Chem. A Mater.* **2021**, *9* (10), 6205–6213. <https://doi.org/10.1039/d0ta11876a>.
- (84) Tamura, M.; Chaikittisilp, W.; Yokoi, T.; Okubo, T. Incorporation Process of Ti Species into the Framework of MFI Type Zeolite. *Microporous Mesoporous Mater.* **2008**, *112* (1–3), 202–210. <https://doi.org/10.1016/j.micromeso.2007.09.044>.
- (85) Guo, Q.; Feng, Z.; Li, G.; Fan, F.; Li, C. Finding the “Missing Components” during the Synthesis of TS-1 Zeolite by UV Resonance Raman Spectroscopy. *J. Phys. Chem. C* **2013**, *117* (6), 2844–2848. <https://doi.org/10.1021/jp310900a>.
- (86) Shan, Z.; Lu, Z.; Wang, L.; Zhou, C.; Ren, L.; Zhang, L.; Meng, X.; Ma, S.; Xiao, F.-S. Stable Bulky Particles Formed by TS-1 Zeolite Nanocrystals in the Presence of H₂O₂. *ChemCatChem* **2010**, *2*, 407–412.
- (87) Bordiga, S.; Lamberti, C.; Bonino, F.; Travert, A.; Thibault-Starzyk, F. Probing Zeolites by Vibrational Spectroscopies. *Chem. Soc. Rev.* **2015**, *44* (20), 7262–7341. <https://doi.org/10.1039/c5cs00396b>.
- (88) Armaroli, T.; Milella, F.; Notari, B.; Willey, R. J.; Busca, G. A Spectroscopic Study of Amorphous and Crystalline Ti-Containing Silicas and Their Surface Acidity. *Top. Catal.* **2001**, *15* (1), 63.
- (89) Wu, L.; Zhao, S.; Lin, L.; Fang, X.; Liu, Y.; He, M. In-Depth Understanding of Acid Catalysis of Solvolysis of Propene Oxide over Titanosilicates and Titanosilicate/H₂O₂ Systems. *J. Catal.* **2016**, *337*, 248–259. <https://doi.org/10.1016/j.jcat.2016.01.028>.
- (90) Pelmeshnikov, A. G.; Santen, R. A. Van; Jánchen, J.; Meijer, E. CD₃CN as a Probe of Lewis and Bronsted Acidity of Zeolites. *J. Phys. Chem.* **1993**, *97*, 11071–11074.
- (91) Zecchina, A.; Marchese, L.; Bordiga, S.; Pazè, C.; Gianotti, E. Vibrational Spectroscopy of NH₄⁺ Ions in Zeolitic Materials: An IR Study. *J. Phys. Chem. B* **1997**, *101*, 10128–10135.
- (92) Giordanino, F.; Borfecchia, E.; Lomachenko, K. A.; Lazzarini, A.; Agostini, G.; Gallo, E.; Soldatov, A. V.; Beato, P.; Bordiga, S.; Lamberti, C. Interaction of NH₃ with Cu-SSZ-13 Catalyst: A Complementary FTIR, XANES, and XES Study. *J. Phys. Chem. Lett.* **2014**, *5* (9), 1552–1559. <https://doi.org/10.1021/jz500241m>.
- (93) Datka, J.; Góra-Marek, K. IR Studies of the Formation of Ammonia Dimers in Zeolites TON. *Catal. Today* **2006**, *114* (2–3), 205–210. <https://doi.org/10.1016/j.cattod.2006.01.009>.
- (94) Signorile, M.; Damin, A.; Bonino, F.; Crocellà, V.; Lamberti, C.; Bordiga, S. The Role of Dispersive Forces Determining the Energetics of Adsorption in Ti Zeolites. *J. Comput. Chem.* **2016**, *37*, 2659–2666. <https://doi.org/10.1002/jcc.24509>.

- (95) Bordiga, S.; Damin, A.; Bonino, F.; Zecchina, A.; Spanò, G.; Rivetti, F.; Bolis, V.; Prestipino, C.; Lamberti, C. Effect of Interaction with H₂O and NH₃ on the Vibrational, Electronic, and Energetic Peculiarities of Ti(IV) Centers TS-1 Catalysts: A Spectroscopic and Computational Study. *J. Phys. Chem. B* **2002**, *106* (38), 9892–9905. <https://doi.org/10.1021/jp026106t>.
- (96) Tozzola, G.; Mantegazza, M. A.; Ranghino, G.; Petrini, G.; Bordiga, S.; Ricchiardi, G.; Lamberti, C.; Zulian, R.; Zecchina, A. On the Structure of the Active Site of Ti-Silicalite in Reactions with Hydrogen Peroxide: A Vibrational and Computational Study. *J. Catal.* **1998**, *179* (1), 64–71. <https://doi.org/10.1006/jcat.1998.2205>.
- (97) Colthup, N. B.; Daly, L. H.; Wiberley, S. E. Ethers, Alcohols and Phenols. In *Introduction to Infrared and Raman Spectroscopy*; Elsevier, 1990; pp 327–337. <https://doi.org/10.1016/b978-0-08-091740-5.50013-2>.
- (98) Hudson, R. L.; Loeffler, M. J.; Yocum, K. M. Laboratory Investigations into the Spectra and Origin of Propylene Oxide: A Chiral Interstellar Molecule. *Astrophys. J.* **2017**, *835* (2), 225. <https://doi.org/10.3847/1538-4357/835/2/225>.
- (99) Goebbel, H.G.; Bassler, P.; Teles, J. H.; Rudolf, P.; Mueller, U.; Forlin, A.; Schulz, M.; Weidenbach, M. Process for Epoxidizing Propene. US Patent 7786317 B2, 2010.
- (100) Haas, T.; Brasse, C.; Woll, W.; Hofen, W.; Jaeger, B.; Stochniol, G.; Ullrich, N. Process for the Epoxidation of Propene. US Patent 6878836 B2, 2005.